https://doi.org/10.5194/egusphere-2026-2767
Preprint. Discussion started: 11 August 2026

Snowpack depth hoar impacts on the permafrost thermal regime in a land surface model

Hotaek Park[1,5], Kazuyoshi Suzuki[2], Steven R. Fassnacht[3], Yoshihiro Iijima[4], Tetsuya Hiyama[5]

[1]Institute of Arctic Climate and Environment Research, JAMSTEC, Yokosuka, Japan
[2] Institute of Arctic Climate and Environment Research, JAMSTEC, Yokohama, Japan
[3] ESS-Watershed Science, Colorado State University, Fort Collins, Colorado, USA
[4] Department of Geography, Tokyo Metropolitan University, Hachioji, Tokyo, Japan
[5] Institute for Space-Earth Environmental Research, Nagoya University, Nagoya, Japan

Correspondence to: Hotaek Park (park@jamstec.go.jp)

Abstract. In cold, dry regions, snowpacks can build a basal depth hoar layer that has a lower density that effectively increases the insulative ability and thus warms permafrost. However, the precise magnitude of the depth hoar insulation and the subsequent impact on permafrost thermal regimes remains highly uncertain. Current Earth and land surface models do not consider the depth hoar effect in their simulations. This study coupled a depth hoar scheme into the snowpack processes within a land surface model. The depth hoar effect on the permafrost thermal regimes in present (1980–2016) and future (2015–2100) climates was assessed by model simulations excluding and including depth hoar. Snow and soil thermal properties observed at the field sites were used to evaluate the model results. The modeling assessment revealed that the depth hoar produced permafrost warming of 2.5–4.0°C in February under the present climate and deepened the active layer thickness by up to 20 cm. The insulative ability of depth hoar was further significant for colder air temperatures and a thicker snowpack. The effect was demonstrated by increased temperature differences between the air and soil depth at 20 cm with increasing snow depth under colder air temperature conditions. Under a future warming climate, the depth hoar functioned as an insulator enhancing permafrost degradation. Our analysis reveals a new perspective on the underlying influence of depth hoar as a driver of permafrost degradation in present and future climates. We recommend improvements to model representation to include the depth hoar process to improve simulations of the permafrost-related changes under warming climate.

1 Introduction

Snow is a critical variable affecting regional climate and hydrology, then amplifying the influence at the global scale. In the Arctic, air temperature has been increasing three times faster than the global mean for the recent few decades (IPCC, 2022), which likely causes changes in snow phenology and processes and their related feedback. Extensive observations show a retreat of snow cover at the Arctic scale (Estilow et al., 2015; Mudryk et al., 2020), earlier onset of snow melting in spring (Mudryk et al., 2017; Park et al., 2024), and a decrease of snow water equivalent (SWE) in the winter, particularly over the North America continent (Pulliainen et al., 2020). These changes can cause modifications of hydrological and thermal

https://doi.org/10.5194/egusphere-2026-2767
Preprint. Discussion started: 11 August 2026

processes in the spring. For example, an earlier snow melting results in an increase in the energy into the soil, advancing spring soil thawing (Park et al., 2015; Kim et al., 2017). Occasionally, a deeper snowpack extends the snow cover period and leads to cooler soil temperatures during the growing season (Walker et al., 1999; Hinkel and Hurd, 2006). However, snow functions as an effective insulator, limiting the cooling of permafrost soil during the winter season. The increase in the winter snow mass enhances the insulation rate and warms permafrost. Field observations identified the increase of snow depth in the eastern Siberia over recent decades (Zhong et al., 2014), which was linked to the permafrost warming (Park et al., 2015) and the deepening of active layer thickness (Park et al., 2013). In contrast, during the same period, the decreased snow depth in the North America Arctic resulted in a shallower active layer thickness (Park et al., 2013), opposite from the warming of air temperature.

In the Arctic tundra environment, the snowpack can be simplified into two parts of a basal depth hoar layer overlain by a wind slab (Sturm et al., 1995; Domine et al., 2012). These two layers have different structures and physical properties. Depth hoar forms from the kinetic metamorphism of snow due to a vapor gradient that is induced by a temperature gradient, typically >10 K m^{-1} (Marbouty, 1980; Colbeck, 1983). The water vapor pressure gradient generates a water vapor flux between the warm basal snowpack and the upper or top layers of the snowpack. The water vapor is delivered upward through the snowpack (Yosida, 1955), resulting in the growth of coarse faceted and striated hollow depth hoar crystals. The temperature gradient is greater at the beginning of the winter season when the snowpack is relatively thin and the ground is still at or near 0°C, while the air temperature is much colder. Depth hoar forms from the initial snow accumulation and usually found at the base of the snowpack throughout the winter season. The depth hoar increases the role for snowpack thermal insulation and therefore for the ground thermal regime and near surface air temperature (Zhang, 2005).

Many land surface models adopted a multilayer snow scheme to represent more specifics of snow properties and their variations (Bartelt and Lehning, 2002; Vionnet et al., 2012; Lawrence et al., 2019). However, models exhibit significant discrepancies in the simulated vertical density profiles compared to observed snow density, in both the top wind slab and bottom depth hoar layer (Dutch et al., 2022). These discrepancies are likely amplifying the anomalies in the simulation for permafrost thermal regimes, created by the variations in the snowpack insulation (Wang et al., 2013; Paquin and Sushama, 2015; Barrere et al., 2017; Slater et al., 2017; Dutch et al., 2022; Damseaux et al., 2025). Land surface models reveal cold biases of the simulated versus observed soil temperature at the Arctic scale (Dankers et al., 2011; Lawrence et al., 2012; Park et al., 2013; Ekici et al., 2014). This demonstrates the inadequate representation of the snow insulative capacity in models as a significant source of the biases (Barrere et al., 2017; Domine et al., 2019; Dutch et al., 2022). To better simulate Arctic snow structure and snow thermal properties, Royer et al. (2021) conducted sensitivity experiments involving parameterizations of several snow physical processes in the Crocus model, showing only slight improvements in soil temperature. Dutch et al. (2022) conducted a comparative analysis of different snow thermal conductivity schemes with CLM5.0 and demonstrated that the snow thermal conductivity scheme proposed by Sturm et al. (1997) mitigates winter soil temperature biases (Paquin and Sushama, 2015; Tao et al., 2024). This result is consistent with the model simulations of Damseaux et al. (2025), who extended the Dutch et al. (2022) assessments to the entire pan-Arctic domain. The work highlights the large sensitivity of soil

https://doi.org/10.5194/egusphere-2026-2767
Preprint. Discussion started: 11 August 2026

temperature to snow thermal conductivity, necessitating improvements in the simulation of observed wintertime soil temperature. However, the incorporation of depth hoar scheme within land surface models is limited, and thus the models have deficiencies in simulating thermal insulation properties of Arctic snowpacks.

The most typical depth hoar crystals form unconsolidated layers of low density (Domine et al., 2018; Damseaux et al., 2025), resulting in lower heat conductivity (λ = 0.025–0.1W m^{-1} K^{-1}) than for the wind slabs (λ = 0.15–0.5 W m^{-1} K^{-1}) (Sturm et al., 1997). The impact of these low-density, low thermal conductivity in depth hoar layers could be substantial to the thermal regimes of permafrost of the Arctic and subarctic (Zhang et al., 1996), since depth hoar can comprise up to 80% of the snowpack (Sturm and Johnson, 1991). However, field observations that evaluate the impacts of depth hoar on soil temperature have been limited due to the experimental difficulty in performing such assesments. A few efforts were made to assess the depth hoar impacts on permafrost thermal regimes with numerical models. Zhang et al. (1996) conducted a sensitivity study in permafrost regions using a one-dimensional finite difference conductive heat transfer model and found that the effective thermal conductivity of snowpacks decreases nonlinearly with increases in the depth hoar fraction and thus warmer soil temperature. Yamazaki (2001) introduced an effective temperature gradient as an index of depth hoar, which was coupled to thermal conductivity and compactive viscosity coefficient in the snow submodel of a land surface model, that reproduced the observed vertical soil temperature profile well at a subarctic larch forest in eastern Siberia. The SNOWPACK model that included a depth hoar factor to calculate the successive change of the snow shear strength during metamorphosis generally simulated snow changes measured in the laboratory experiments using artificial snow (Hirashima et al., 2008). However, modeling the depth hoar process is still in its early stages.

Modeling studies have projected a general trend towards a shorter snow season and reduced snow extent under future climate change (Mudryk et al., 2020; McCrystal et al., 2021; Zhu et al., 2021). The latest generation of climate models (CMIP6, the Coupled Model Intercomparison Project, phase 6) show an even more rapid snow-to-rain transition by the end of 21st century than previous model generations (McCrystal et al., 2021). O'Gorman (2014) found that the occurrence of extreme snowfall increases with warming due to increasing atmospheric water vapor, offsetting the snow loss induced by temperature warming. The increasing winter snow mass likely insulates more thus reducing the cooling of the soil in the winter that accelerates the permafrost warming, and combined warmer air temperature, causes earlier-than-expected losses of climate-warming legacy carbon from permafrost (Pongracz et al., 2024). The simulation results from CMIP6 also include biases due to model deficiency in not representing the effects of depth hoar (Luo et al., 2025). There is a lack of understanding of how much depth hoar induced insulation contributes to the permafrost temperature in present and future climates.

The main goal of this study is to quantify the contribution of depth hoar as snow insulation to the permafrost thermal regime, tested at a boreal larch forest in eastern Siberia. This builds upon simulations of the coupled hydrological and biogeochemical model (CHANGE, Park et al., 2011, 2018, 2021) that incorporates the depth hoar scheme of Yamazaki (2001) into the snow component of CHANGE. Specifically, two model simulations were conducted (including and excluding depth hoar) to assess impacts of the depth hoar on snow density and thermal conductivity, and thus soil temperature. The simulation results were compared to the observations for the period from 1980 to 2016 to evaluate model performance. To assess the

https://doi.org/10.5194/egusphere-2026-2767
Preprint. Discussion started: 11 August 2026

impacts of depth hoar on permafrost temperature under the future climate change, model simulations were extended to 2100, forced by meteorological data from a climate model that participated in CMIP6.

2. Method

2.1 General description of CHANGE

The CHANGE model (Park et al., 2011, 2018, 2021) is a process-based land surface model that simulates water, heat, and carbon fluxes, and plant phenology and physiology in the terrestrial ecohydrological system coupling with a vegetation dynamic model. The model simulations provide insight into the responses of the ecosystem processes to climatic forcings, as well as interaction and feedback between the terrestrial surface and atmospheric systems. CHANGE simulates the seasonal variability of snowpack accumulating and melting on the land surface, and the partition of the melted water into surface runoff and soil infiltration (Park et al., 2024, 2026). The infiltrated snow and rain waters flux up and/or down along water pressure gradients between soil layers, in which transpiration and drainage enhance the soil water flux. CHANGE explicitly simulates permafrost dynamics considering the soil freezing/thawing phase change in a soil column of a 50-m depth, based on hydraulic and thermal principles that include both permafrost blocking effect on water flow and the effect of soil organic carbon on the soil hydraulic and thermal properties (Park et al., 2015). The frozen soil layers decrease soil water availability by plant roots, thus increasing the probability of soil water stress. CHANGE includes a water stress parameter encountered by plants for drying and/or freezing conditions, which is coupled to the processes of leaf photosynthesis and stomatal conductance, and sequentially affecting carbon and nitrogen cycles in vegetation and soil biogeochemical processes. CHANGE prognostically simulates carbon and nitrogen state variables in the vegetation, litter, and soil organic matter, including the flow tracks of carbon and nitrogen to leaf, live stem, dead stem, live and dead coarse root, fine root, and grain pools. The seasonal timing of vegetation phenology, including initiation of leaf onset and litterfall, is also prognostic, responding to air and soil temperature, soil water availability, and daylength. The model-estimated leaf and stem area index, root amount, and plant heights are utilized by the biophysical module that simulates water and energy fluxes.

2.2 Snow model

2.2.1 General description

The original snow scheme within CHANGE was a single-layer, energy and mass balance model that simulates snow accumulation and melt incorporating prognostic equations for snow albedo, density and ice and liquid water contents. The model simulations showed overall performance capturing seasonal and interannual variability of observed snow depth and density at different climates and landscapes (Park et al., 2013, 2015). The density and liquid water content of snowpack can have vertically heterogeneous profiles due to snow compaction, water drainage, and energy gradients. Using a process-based multilayer model is expected as a realistic approach to give better simulation. In this study, the snow scheme of CHANGE is modified to a multilayer approach, in which the energy and mass balance principles, including albedo, are consistent with the original model. However, the new multilayer snow scheme includes the depth hoar process; this paper describes the related processes.

The snow scheme consists of a maximum of five snowpack layers (d_z, z = 1, 2, .., 5 labelled from the top down). The thickness of the upper four layers is set as a constant by the user; here they are prescribed at 2, 5, 10, and 20 cm. The bottom layer (d_5) of snowpack has a variable thickness. When snow depth (d_s) is shallower than the first-layer thickness of 2 cm, the shallow snow cover is defined as a zero-snow layer that is combined with surface soil layer for numerical stability (Best et al., 2011) and there is no snow insulation. A residual in the surface energy balance is used to melt the shallow snow, which simultaneously forces the soil surface as the heat flux. The melted water is immediately partitioned into surface runoff and soil infiltration without refreezing. When $d_s > d_1$, the ground is covered in snow, and thus the model's snow scheme operates to represent snow processes. As the snow depth increases, the lowest layer of the snowpack increases until the thickness reaches twice its prescribed thickness, then the layer splits in two with the upper layer staying fixed in thickness and the new lower layer thickening as the snow accumulates. As the fifth layer is formed, the snow thickness increases only in that layer. This treatment is reversed as the snow depth decreases, with layers being progressively combined at the bottom of the snowpack. The snow scheme uses a variable snow density for each layer, changing due to metamorphism, ablation, and the accumulation of new snow.

2.2.2 Snow density

Two schemes are available within CHANGE for the representation of the snow density in each layer. The original scheme represents the snow density related to viscous compaction, based on the measurement of Kojima (1967). The state variables in each snow layer consist of thickness (d_z, m), mass of liquid water ($w_{l,z}$, kg m^{-2}), ice content ($w_{i,z}$, kg m^{-2}), density (ρ_z, kg m^{-3}), and temperature (T_z, K). In a snow layer, the mass of ice and liquid water is preserved by $\rho_z \cdot d_z = w_{l,z} + w_{i,z}$. Snow compaction by snow load or pressure and melting increases the layer density. The change in a snow-layer density over a timestep (t) is calculated as

$$\frac{\partial \rho_z}{\partial t} = \frac{\rho_z g M_z}{\eta_0} \exp\left(\frac{k_s}{T_m} - \frac{k_s}{T_z} - \frac{\rho_z}{\rho_0}\right) \tag{1}$$

where η_0 is compactive viscosity (= 10^7 Pa s), g is gravity, M_z is the mass of snow above the middle layer ($= 0.5\left(w_{i,z} + w_{l,z}\right) + \sum_{i=1}^{z-1}\left(w_{i,i} + w_{l,i}\right)$), T_m is melting temperature (= 273.15 K), k_s = 4000 K, and ρ_0 is reference density (= 50 kg m^{-3}). The ice content and liquid water are used to calculate the areal heat capacity of the snow layer. The snow density estimated by Eq. (1) is parameterized for the calculation of heat conductivity (λ_z, Jordan, 1991) as

$$\lambda_z = \lambda_{air} + (7.75 \times 10^{-5}\rho_z + 1.105 \times 10^{-6}\rho_z^2) \times (\lambda_{ice} - \lambda_{air}) \tag{2}$$

where λ_{ice} and λ_{air} are the thermal conductivity of ice (= 2.29 W m^{-1} K^{-1}) and air (= 0.023 W m^{-1} K^{-1}), respectively.

2.2.3 Depth hoar

https://doi.org/10.5194/egusphere-2026-2767
Preprint. Discussion started: 11 August 2026

The new scheme includes the effect of depth hoar on snow density, which is based on the algorithm developed by Yamazaki (2001). Depth hoar forms toward the base of snowpack. Depth hoar crystals have highly faceted, unconsolidated, and often cup-shaped grains with low density (Sturm et al., 1997), which grows in snowpack with temperature gradients larger than >10°C m^{-1} (Colbeck, 1983). The crystal growth rate depends on temperature gradient (Γ), diffusion coefficient of water vapor (D_v), differential coefficient (δ) of temperature-related saturated vapor density, and snow particle size. The values of D_v and δ are proportional to temperature. Higher temperature generally increases the growth of depth hoar crystals. The effective temperature gradients (g_t) from temperature dependent parts are described as

$$\left.\begin{array}{ll} g_t(z,t) = \Gamma f(T_z) & (\Gamma \geq 10℃\,\mathrm{m}^{-1}) \\ g_t(z,t) = 0 & (\Gamma < 10℃\,\mathrm{m}^{-1}) \end{array}\right\} \tag{3}$$

where $\Gamma = |\partial T_z / \partial z|$ and

$$f(T_z) = \frac{D_v(T_z)}{D_v(T_0)} \frac{\delta(T_z)}{\delta(T_0)}$$

$$\simeq 1 + 0.0733T_z + 0.00197T_z^2 + 0.0000187T_z^3 (-40℃ \leq T_z \leq 0℃, T_0 = 0℃).$$

An index of depth hoar formation (G_t) is represented by the integration of g_t as

$$G_t(z, t + \Delta t) = G_t(z,t) + g_t \Delta t. \tag{4}$$

Here, the values of G_t and depth hoar are reset to zero at the state that the liquid water content exceeds 90% of the maximum water amount (= $w_{lmax,z}/\rho_z$, 0.1) for a snow layer, which is because the depth hoar has already collapsed at the saturated condition. As the value of G_t reaches a threshold, it is combined with compactive viscosity coefficient and thermal conductivity. The viscous compression of the snow layer is represented as

$$\frac{\partial \rho_{dry}}{\partial t} = \frac{W}{\eta} \rho_{dry} \tag{5}$$

where ρ_{dry} is the dry density of snow (= $\rho_z - \rho_{liq,z}$), W is overburden snow load, and η is the compactive viscosity coefficient. Yamazaki et al. (1993) introduced an equation on the compactive viscosity coefficient excluding depth hoar (η_{ndh}) as follows:

$$\eta_{ndh} = \alpha_v \eta_{dh0} \exp(K\rho_{dry} - \alpha_s T_z) \tag{6}$$

where η_{dh0}=6.9×10^5 kg s m^{-2}, K=2.1×10^{-2} m^3 kg^{-1}, and α_s=9.58×10^{-2} °C^{-1} are constants (Kojima 1957; Shinojima 1967). α_v describes the decrease of the compactive viscosity coefficient caused by liquid water, assumed as

$$\alpha_v(w_{l,z}) = \frac{\exp(-\beta_s w_{l,z}) - \exp(-\beta_s)}{1 - \exp(-\beta_s)} \tag{7}$$

where β_s is a constant (=18).

The compactive viscosity coefficient of depth hoar (η_{dh}) is larger than the value of rounded grains under the same density. Therefore, it is assumed that the value of η_{dh} is linearly increased dependent on G_t (Eq. 4) as

$$\left.\begin{array}{ll} \eta_{dh} = \eta_{ndh} & (G_t < G_{t0}) \\ \eta_{dh} = \frac{(f_v - 1)G_t + G_{tv} - f_v G_{t0}}{G_{tv} - G_{t0}} \eta_{ndh} & (G_{t0} \leq G_t < G_{tv}) \\ \eta_{dh} = f_v \eta_{ndh} & (G_{tv} \leq G_t) \end{array}\right\} \tag{8}$$

https://doi.org/10.5194/egusphere-2026-2767
Preprint. Discussion started: 11 August 2026

where G_{t0} = 1×10^7 °C m^{-1} s (= 1.2 °C cm^{-1} day), G_{tv} = 4×10^7 °C m^{-1} s (= 4.8 °C cm^{-1} day), and f_v = 10 are constants. The constant values were determined by field or laboratory experiments (Kojima, 1956; Fukuzawa and Akitaya, 1991). G_{t0} has the value of G_t, as the depth hoar begins to form. The formation of the depth hoar decreases the thermal conductivity (λ) of the snow layer, which is expressed by the similar equations used in the compactive viscosity of Eq. (8) as

$$\left.\begin{array}{ll} \lambda = \lambda_z & (G_t < G_{t0}) \\ \lambda = \frac{(f_t-1)G_t + G_{tt} - f_t G_{t0}}{G_{tt} - G_{t0}} \lambda_z & (G_{t0} \le G_t < G_{tt}) \\ \lambda = f_t \lambda_z & (G_{tt} \le G_t) \end{array}\right\} \quad (9)$$

where G_{tt} = 1×10^8 °C m^{-1} s (=12 °C cm^{-1} day) and f_t = 0.3. λ_z of the right-hand side in Eq. (9) is calculated by Eq. (2).

2.2.4 Snow temperature and hydrology

In the multilayer snow scheme, the temperature of a snow layer is calculated based on the heat fluxes inflowing from the upper layer and outflowing to the lower layer, thickness, and heat capacity with fully implicit forward timestep weighting. For the lowest snow layer, the thermal conditions of surface soil layer are combined for the calculation of both the snow temperature of the bottom layer and heat flow to the soil. If the temperature of a snow layer is calculated to be warmer than T_m (= 273.15 K), the layer ice mass is reduced as

$$\Delta w_{i,z} = \frac{C_z}{L_f}(T_z - T_m) \quad (10)$$

where C_z is the areal heat capacity of the layer (J kg^{-1} K^{-1}) and L_f is the latent heat of fusion (J kg^{-1}). The melted ice amount is added to the layer liquid water and the layer temperature is set to T_m. When the liquid water of a snow layer exceeds the capacity (= $\rho_{\mathrm{liq}} \cdot d_z$), the excess water is passed to the layer below. Liquid water in a snow layer with a temperature colder than T_m will refreeze, decreasing the liquid content as

$$\Delta w_{l,z} = \frac{C_z}{L_f}(T_m - T_z) \quad (11),$$

increasing the ice content by the same amount, which is also related to a decrease in the layer temperature. The liquid water flux at the bottom layer of snowpack is passed to surface soil layer. A new snow is added to the first layer with the density of 150 kg m^{-3} and temperature is equal to the snow surface layer temperature, in which sublimation calculated by the surface energy exchange is removed from the surface layer ice mass and from lower layers if the surface layer sublimates entirely during the timestep. Then, the snow layers are combined or split to match the fixed layer thicknesses, as described above. In the reorganized snow layers, the ice and liquid water masses are conserved by the mass balance and their temperature is diagnosed by the energy balance.

2.3 Study site and observation

The observation site, underlain with continuous permafrost, is located at approximately 20 km north of Yakutsk in eastern Siberia (Fig. 1a). The site, which is called "Spasskaya Pad" (Kotani et al., 2019), is operated as an experimental forest of the Institute for Biological Problems of Cryolithozone, Siberian Branch of the Russian Academy of Sciences (SB-RAS).

https://doi.org/10.5194/egusphere-2026-2767
Preprint. Discussion started: 11 August 2026

Climatologically, the site recorded a seasonal daily mean air temperature range of −50 to 30°C and low annual precipitation of approximately 200–300 mm during the period of 1998–2014. The forest overstory is dominated by 180-year old larch trees (*Larix cajanderi*), mixed with birch (*Betula pendula*) and willow (*Salix bebbiana*) (Fig. 1b). The forest floor is fully covered by dense cowberry (*Vaccinium vitis-idaea*). In recent years, young willow trees have grown to form an understory canopy layer with younger birch trees. The soil at the experimental site is classified as sandy loam, and the surface is covered by a thicker litter layer of approximately 10 cm. The surface soil of permafrost thaws during the warm season, and the melt water is an important soil water resource for plants. The seasonal maximum active layer thickness (ALT) was lower than 1.5 m prior to 2004 but recently increased to deeper than 2 m. A full description of the site is given in Kotani et al. (2019).

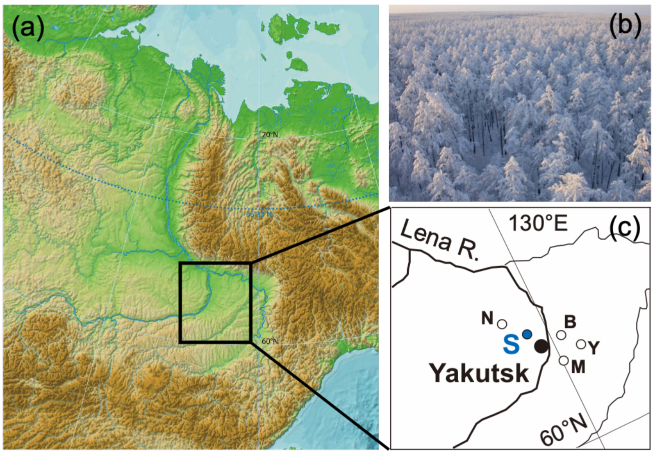

Figure 1. The study area showing (a) the topography in northeastern Siberia, including Yakutsk region in the main map, (b) snow-covered landscape in the study site of Spasskaya Pad, and (c) soil temperature and active layer thickness observation sites in the Yakutsk area (S: Spasskaya Pad, N: Nelger, B: Bestyakh, M: Maya, Y: Yukechi) in the inset map.

A 32-m tall meteorological tower was installed at the site, where various meteorological variables were measured at multiple heights. Eddy-covariance systems were installed at the top of the tower and at the height of 2 m above the forest floor to monitor sensible heat, latent heat, and CO_2 fluxes. Soil moisture and temperature were measured at multiple depths (0.1, 0.2, 0.4, 0.6, 0.8, and 1.2m) in the soil column. Precipitation was recorded in an open place 1 km south of the tower site during the warm season from the end of April to the end of October. The precipitation measurement during the cold season was discontinued. The gap was filled by observations at the Yakutsk station of the Russian Federal Service for Hydrometeorology and Environmental Monitoring (Roshydromet). The Roshydromet also monitored the seasonal variability of snow depth and snow water equivalent (SWE) at both open and forest sites close to the meteorological station, with a monthly frequency in the early snow season until December and then every 5- or 10-days into early May when the snow disappeared. Snow depth was measured each 10 m along a 500-m snowcourse in the forest, and SWE was made at every 200 m along a 2000-m snowcourse (Zhong et al., 2014). The Melnikov Permafrost Institute, Siberian Branch of Russian Academy of Science (MPI)

https://doi.org/10.5194/egusphere-2026-2767
Preprint. Discussion started: 11 August 2026

has monitored ALT at 16 sites with different landscapes over Yakutsk since 1998 (Fig. 1c, Iijima et al., 2016). The observed ALT, soil temperature, and snow depth were used for evaluating the performance of the modified model.

2.4 Model simulation

The daily model forcing data for the period 1980–2016 were created by the combination of the observed meteorological records at the study site and ERA-Interim reanalysis data from the European Centre for Medium-Range Weather Forecasts. The latter includes the Global Precipitation Climatology Project precipitation dataset and the bias-corrected monthly Climate Research Unit temperature dataset, which were used as the baseline to construct the meteorological forcing data for CHANGE simulations. The generation of the forcing data is fully described by Miyazaki et al. (2015).

To diagnose the impact of the depth hoar on soil thermal properties, the CHANGE model performed two simulations, including depth hoar (Ex_{DH}) and excluding depth hoar (Ex_{NODH}) driven by the daily meteorological forcing data using the same parameterizations and options. The difference on the targeted analytic variables between the two simulations is derived as the impact of the depth hoar.

A static land cover type of boreal deciduous needleleaf forest was prescribed for the CHANGE simulation, while the vegetation phenology was prognostically estimated based on the simulated carbon and nitrogen amounts and soil hydrothermal conditions. Measured fractions of sand, silt, and clay were set initially to those of the vertical soil texture profile, and the soil organic carbon profile was simulated by CHANGE at each time step. Based on these soil properties, CHANGE estimated the thermal and hydraulic properties of the soil. CHANGE determined a dynamic equilibrium of total ecosystem carbon and nitrogen contents with the prescribed climate, through a spin-up repeating for 1200 years using the detrended forcing data of the initial 20 years and a CO_2 concentration of 350 ppm. After completing the spin-up, CHANGE conducted the designed simulations with the daily meteorological forcing data and the observed global atmospheric CO_2 concentration.

The climate at the experimental site showed trends consistent with global warming, warming air temperature and increasing precipitation for recent decades (Park et al, 2024). The phenology and physics of snow are sensitive to the warming climates. To diagnose the influence of the warming climates on depth hoar and, consequently, on the soil thermal regime, we additionally conducted future projections using a forcing data from 2015 to 2100. The forcing data was obtained from the data archive provided by The Inter-Sectoral Impact Model Intercomparison Project (ISIMIP) that created datasets of a global 0.5° latitude/longitude spatial resolution and daily time step for the simulation of land surface models, based on the projection simulation result of a climate model (i.e., IPSL, https://doi.org/10.48364/ISIMIP.842396.1) with the strongest emission scenario, SSP 5.8.5 (Shared Socioeconomic Pathways) of CMIP6 (Coupled Model Intercomparison Project Phase). The meteorological variables of a grid point closest to the experimental site (60.25°N, 120.25°E) were chosen from the global datasets. Using the forcing dataset, two simulations were conducted following the same method designed in the present climate simulations, i.e., including depth hoar and excluding depth hoar.

https://doi.org/10.5194/egusphere-2026-2767
Preprint. Discussion started: 11 August 2026

3 Result

3.1.1 Snow depth and snow water equivalent

Results for snow depth and SWE in the two simulations of $Ex_{\_DH}$ and $Ex_{\_NODH}$ were averaged at a daily time step for the period of 2006–2016 when there were fewer missing data to compare with the observations taken at 5- to 10-day intervals (Fig. 2). In the early winter when snow begins to accumulate, the two simulations produced similar results for snow depth and SWE and showed good agreements with the observations (Fig. 2). Snow depth showed differences between the two simulations beginning in the middle of November until the start of snowmelt, where the observation fell between the two simulations (Fig. 2a). The largest difference of 15 cm was at the end of March when the snow depth reached its maximum. Meanwhile, SWE showed smaller difference between the two simulations during the snow season, and in good agreement with the observation (Fig. 2b). The comparisons indicated that $Ex_{\_DH}$ simulated larger snow depth and SWE than $Ex_{\_NODH}$ over the entire snow season. The simulated snow depth and SWE exhibited seasonal and interannual (Figure S1) variability similar to the observations. However, the largest difference between the simulations and observations is in spring when snow melts, when the model represented earlier snow melting than the observations (Fig. 2). The deviation seems to be related to both the difference in forests for the observation and simulation and the influence of large residual in the energy balance forcing snowmelt, which will be discussed in the section 4.3.

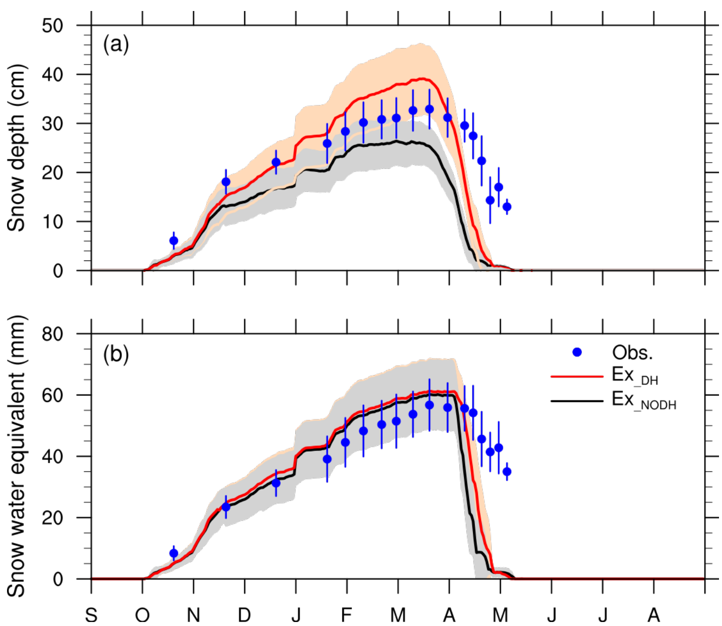

Figure 2. Comparison of the model simulated (a) snow depth and (b) snow water equivalent with depth hoar (red) and without (no) depth hoar (black) to the observations (dots), averaged for the period of 2006–2016. The vertical lines denote one standard deviation of the observation, and shading also denotes the standard deviation for each model experiment.

https://doi.org/10.5194/egusphere-2026-2767
Preprint. Discussion started: 11 August 2026

3.1.2 Soil temperature

The observed and simulated soil temperatures were averaged to three soil depth levels (i.e., 0–30, 30–70, and 70–130 cm), weighing the observed and simulated soil layers' thickness to each depth level, at daily time scale during the period of 2006–2016 that the observational data were available. The model generally simulated the seasonal variability of the observed soil temperature well at the three depth levels (Fig. 3). However, the two simulations of Ex_$_{\mathrm{DH}}$ and Ex_$_{\mathrm{NODH}}$ exhibited cold biases, identified by similar amplitudes of mean absolute deviation (MAD) and root mean square error (RMSE) across all seasons and depths. The cold bias was particularly significant in the early winter, when the model inadequately simulated the observed zero curtains, consistently at the three depth levels. The cold bias was largest at the 70–130 cm level (Fig. 3c) then the 30–70 cm layer (Fig. 3b) and smallest in the uppermost layer (0–30 cm; Fig. 3a). On the other hand, Ex_$_{\mathrm{DH}}$ reduced the cold bias compared to Ex_$_{\mathrm{NODH}}$, as the winter progressed. The depth hoar impact was mostly significant in the mid-winter season, particularly February and March, when Ex_$_{\mathrm{DH}}$ resulted in up to 5–5.5°C warmer soil temperature at the three depth levels than Ex_$_{\mathrm{NODH}}$. Interestingly, the impact of depth hoar on soil temperature was found even at the summer season when Ex_$_{\mathrm{DH}}$ simulated warmer soil temperature than Ex_$_{\mathrm{NODH}}$.

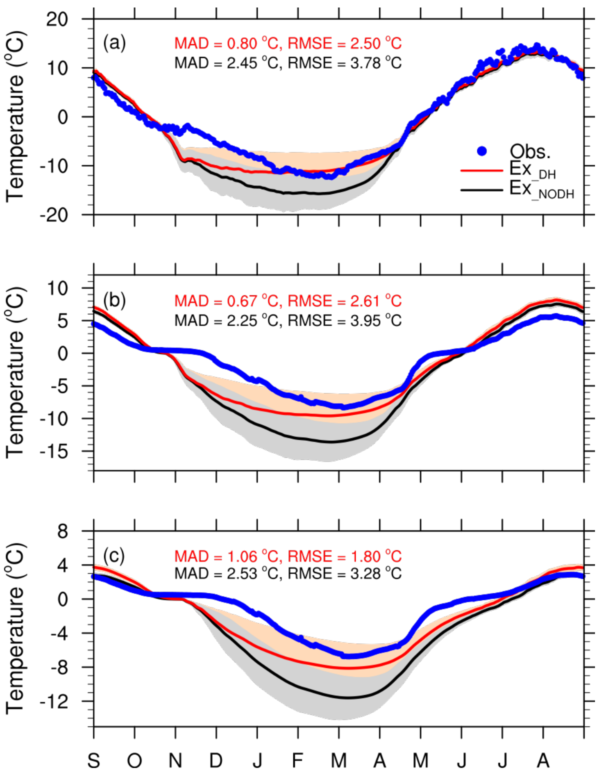

Figure 3. Comparison of the simulated daily soil temperatures at three soil depths (a: 0–30 cm, b: 30–70 cm, c: 70–130 cm) with depth hoar (red) and without (no) depth hoar (black) to the observations (dots), averaged for the period of 2006–2016. The values (MAD, RMSE) represent the performance of each simulation against the observation in the targeted period. Shading denotes the standard deviation for each simulation.

https://doi.org/10.5194/egusphere-2026-2767
Preprint. Discussion started: 11 August 2026

3.1.3 Active layer thickness

The model-simulated ALTs were compared with observations performed at the study site of Spasskaya Pad and various landscapes of 16 sites surrounding Yakutsk. The model simulated the interannual variability of the observed ALT statistically well during the period of 1998–2016 (Fig. 4). The model performance was demonstrated by the higher correlation coefficients, for example, r=0.75 (p<0.01) in Ex$_{_DH}$ and Spasskaya Pad and r=0.72 (p<0.01) in Ex$_{_DH}$ and mean of 16 sites (Fig. 4). The observed ALTs generally distributed between the range of Ex$_{_DH}$ and Ex$_{_NODH}$. Ex$_{_DH}$ recorded the largest ALT of 161 cm, which was larger 16.6 cm than Ex$_{_NODH}$, indicating the effect of soil temperature memory warmed by the depth hoar. The observations and simulations consistently showed the increasing trends of ALT with the amplitude of 0.31 cm yr^{-1} (p<0.42) to 1.12 cm yr^{-1} (p<0.012) under warming air temperatures.

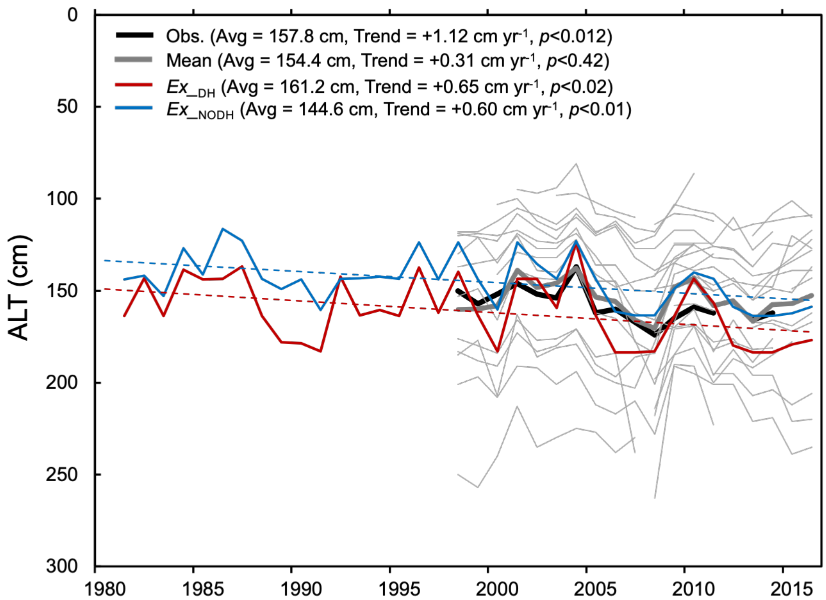

Figure 4. Comparison of the simulated active layer thicknesses to observations. The black is the active layer thickness observed at the study site, Spasskaya Pad, and thick grey is the averaged value for the observations (thin grey) conducted at various landscapes around Yakutsk.

3.2 Seasonal variation of snow grain form

The snow that fell in the early snow season metamorphized to faceted particles starting in the middle of October, which then developed to depth hoar at the bottom layer of the snowpack in November (Fig. 5). The growth of the depth hoar layer continued into March, when the thickness of depth hoar reached a maximum of 43 cm. The time series of snow grains showed that the depth hoar layer tended to grow with a deepening snowpack. As the snowpack becomes deeper, the depth hoar also grows due to a vapor gradient that is induced by a temperature gradient. Meanwhile, depth hoar grains are rapidly metamorphized into rounded grains with snow melting in April.

https://doi.org/10.5194/egusphere-2026-2767
Preprint. Discussion started: 11 August 2026

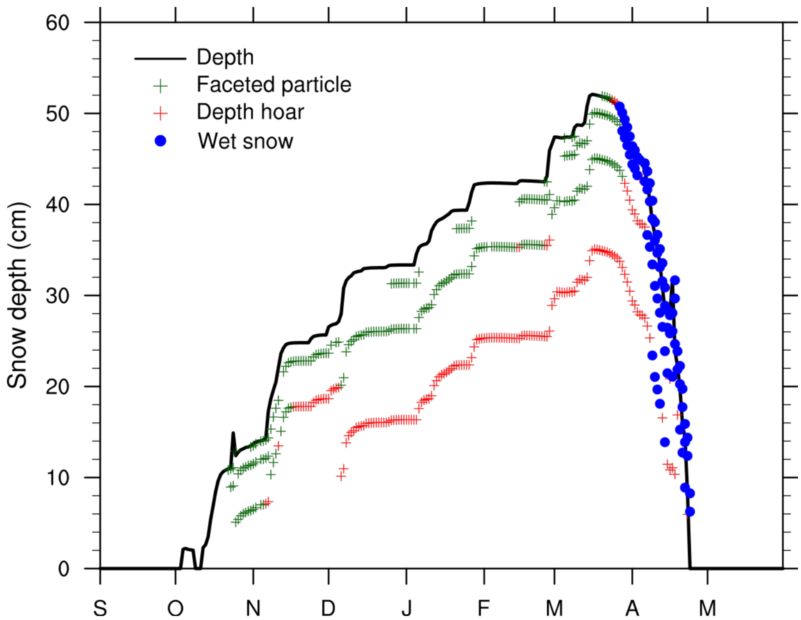

Figure 5. Seasonal variations of simulated snow types: wet snow (w>0.01), depth hoar ($G_t > 4 \times 10^7$ °C m^{-1} s), and faceted particle (1×10^7 °C m^{-1} s $< G_t < 4 \times 10^7$ °C m^{-1} s). The snow types were defined by Yamazaki (2001).

3.3 Depth hoar impacts on snow density and snow thermal conductivity

The vertical profiles of snow density simulated by Ex$_{DH}$ and Ex$_{NODH}$ were averaged to monthly values over the study period. This analysis was also consistently applied to snow thermal conductivity. Figure 6 compares the averaged snow density profiles of the two simulations for the different four months (e.g., October, December, February, and April). The modeled density increases with depth for the Ex$_{NODH}$ simulation in each month, but not for Ex$_{DH}$ (Fig. 6). For example, Ex$_{DH}$ resulted in the profiles where snow density slightly decreased from the top layer toward the bottom as shown in October and April or showed vertically similar values of approximately 150 kg m^{-3} in December and February. Meanwhile, the snow density in Ex$_{NODH}$ increased toward the bottom layer of snowpack, showing differences of approximately 100 kg m^{-3} between the top and bottom layers in December and February (Figs. 6b and 6c). During the mid-winter, a difference 100 kg m^{-3} was also found between the bottom layer of Ex$_{NODH}$ and the same depth of Ex$_{DH}$, representing the impact of depth hoar. In April when relatively wet snowfall and snowmelt at the top layers occurred, the wet snow of high density covered the top layers; here the snow density decreased downward consistently in both Ex$_{DH}$ and Ex$_{NODH}$ (Fig. 6d). However, the difference in snow density between the two simulations still large at the lower layers.

The simulated vertical snow heat conductivity was larger at the base of the snowpack for Ex$_{NODH}$ compared to Ex$_{DH}$ (Fig. 7). This difference increased as the winter season progressed. The thermal conductivity of Ex$_{DH}$ produced lower values in the vertical profiles than Ex$_{NODH}$ for all months. In Ex$_{DH}$, the depth hoar formed at the lower layers (Fig. 5) resulted in

https://doi.org/10.5194/egusphere-2026-2767
Preprint. Discussion started: 11 August 2026

evidently lower thermal conductivity of on average <0.1 W m^{-1} K^{-1} than the surface layers in all months. Meanwhile, the snow thermal conductivity in Ex$_{\text{NODH}}$ showed different profiles in the months. In October and April, the snow thermal conductivity decreased toward the bottom layer, which was attributable to relatively fresh and wet snow that was existent at the top layers and had higher thermal conductivity. In contrast, the snow thermal conductivity of Ex$_{\text{NODH}}$ in December and February increased toward the bottom layers where the snow density was larger (Fig. 6), caused by overburden snow compaction.

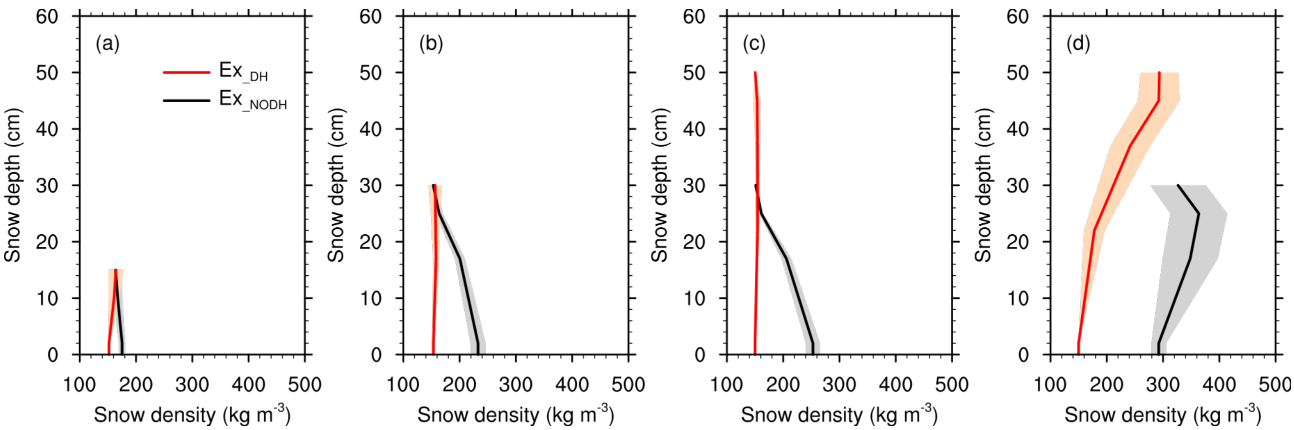

Figure 6. Comparison of the vertical snow density between two simulations in different months, (a) October, (b) December, (c) February, and (d) April, averaged for the study period (1980–2016). Shadings denote the standard deviation, and 0 cm of snow depth represents soil surface.

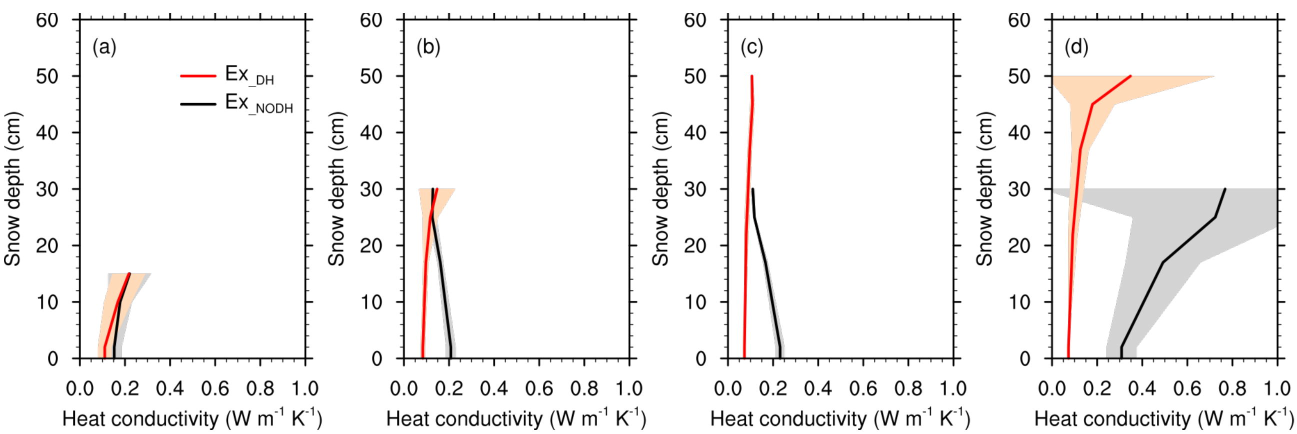

Figure 7. Comparison of the vertical snow heat conductivity between two simulations in different months, (a) October, (b) December, (c) February, and (d) April, averaged for the study period (1980–2016). Shadings denote the standard deviation, and 0 cm of snow depth represents soil surface.

https://doi.org/10.5194/egusphere-2026-2767
Preprint. Discussion started: 11 August 2026

3.4 Correlation between air-soil temperature difference and snow depth

The simulation demonstrates higher snow insulation by the depth hoar at the study site. The snow insulation effect was quantitatively analyzed by the methodology outlined by Wang et al. (2016). The simulations exhibited similar behaviors for air–soil temperature difference (ΔT) in three individual T_{air} regimes, showing larger ΔT under colder T_{air} conditions. The magnitude of ΔT was larger in Ex_DH (Fig. 8b) than in Ex_NODH (Fig. 8a) under individual T_{air} conditions, representing higher snow insulation ability of depth hoar. In the two simulations, ΔT was consistently most notable under the coldest T_{air} condition T_{air}≤–25°C, in which ΔT linearly increased up to 20 cm in snow depth and stabilized thereafter. Meanwhile, ΔT in the different two T_{air} regimes showed different behaviors compared to the coldest T_{air} regime. In the warmer T_{air} regimes, ΔT showed complex responses to the change of snow depth; ΔT recorded the minimal values at the snow depth of 15 cm or 20 cm and then increased with the snow depth. The negative correlation of ΔT to snow depth at relatively shallow snow depth, d_s<20 cm, likely represents the influence of model bias for soil temperature at the early snow season (Fig. 3) and weaker snow insulation at snowmelt timing.

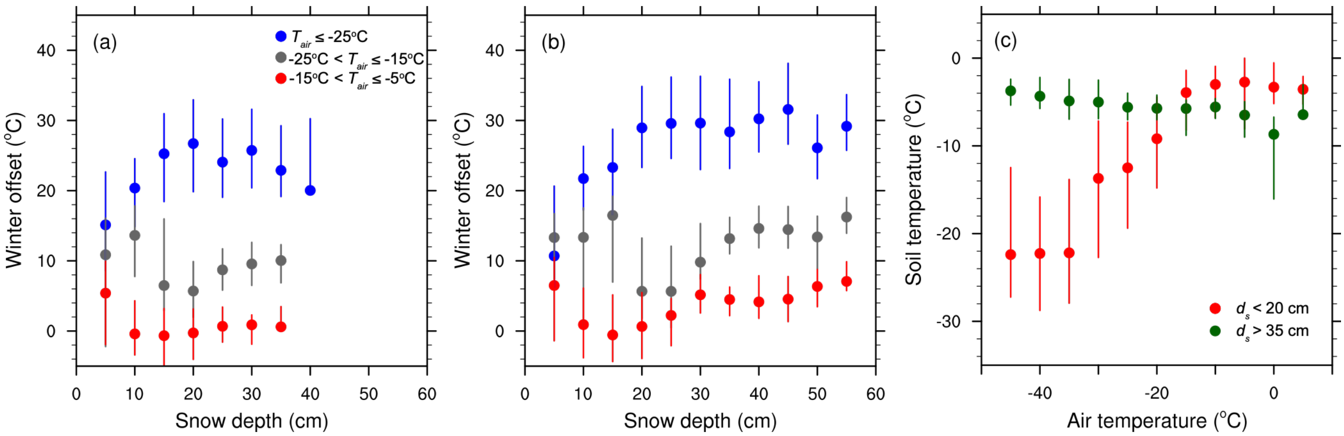

Figure 8. Variation of ΔT (°C), the difference between soil temperature at 20 cm depth and air temperature with snow depth (cm) for winter 1980–2016. The dots represent the medians of 5 cm snow depth bins at different air temperature regimes and the upper and lower lines indicate the 25th and 75th percentiles, calculated for winters of the study period in the simulation of (a) Ex_NODH and (b) Ex_DH. (c) shows variation of soil temperature at 20 cm depth (°C) with air temperature (°C) for winters of the study period under different snow depth regimes, calculated from the simulation of Ex_DH, in which the dots represent the median of 5°C air temperature bins and the upper and lower lines indicate the 25th and 75th percentiles, calculated for winters of the study period in the simulation of and Ex_DH.

The snow insulation capacity is in turn demonstrated by the correlation of soil temperature at 20 cm depth with T_{air}, separated by shallow (d_s<20 cm) and thick (d_s>35 cm) snow conditions based on the result of Ex_DH (Fig. 8c). The soil temperature showed different sensitivity to T_{air} changes at the two snow conditions. At the shallow snowpack (d_s<20 cm), the soil temperature linearly responded to the change of T_{air}, which was identified by the higher regression slope between soil temperature and T_{air} of 0.47 °C °C^{-1} (r=0.94, p<0.01), which was larger than -0.07 °C °C^{-1} (r=0.86, p<0.01) for the thick

https://doi.org/10.5194/egusphere-2026-2767
Preprint. Discussion started: 11 August 2026

snowpack (d_s>35 cm). Meanwhile, the soil temperature under the thick snow condition showed smaller variability to the changes of T_{air}, emphasizing the reduced sensitivity of soil temperature to T_{air} under thick snow conditions.

The correlation of ΔT and T_{air} is represented by a complementary form using conditional probability density functions (PDFs) of ΔT for different T_{air} regimes (Fig. 9). The modal value and width of PDFs reflect the sensitivity of ΔT dependent on T_{air} condition. Figure 9 clearly shows separated ΔT regimes under different T_{air} conditions. The modal values of ΔT PDFs in the three T_{air} regimes were larger in Ex_DH than in Ex_NODH and in cold T_{air} than in warm. The width of PDFs became larger as T_{air} cools. The larger modal value and width of ΔT PDFs under cold T_{air} indicate the influence of T_{air} on snowpack properties, particularly snow density and moisture content that affect the snow thermal conductivity (Wang et al., 2016).

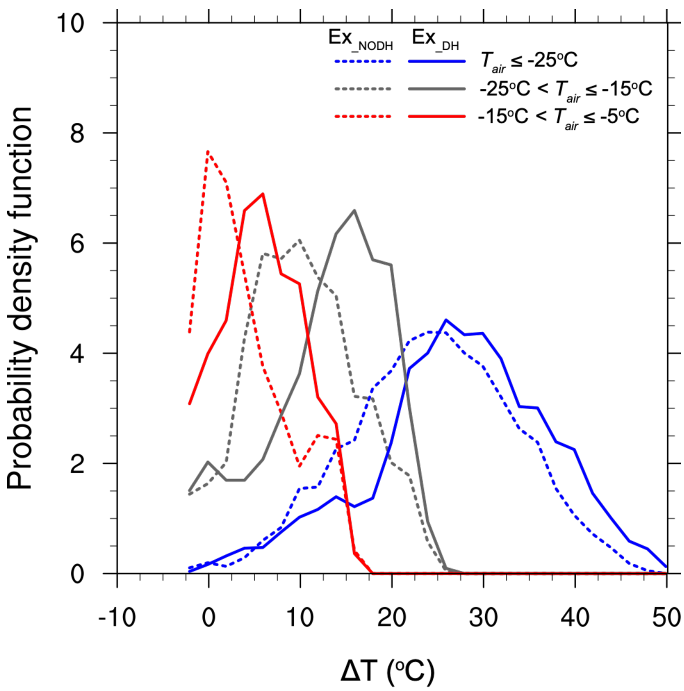

Figure 9. Conditional probability density functions (PDFs) of ΔT (°C), the difference between soil temperature at 20 cm depth and air temperature for different air temperature regimes for winters of the study period in the simulations of Ex$_{_NODH}$ and Ex$_{_DH}$.

4. Discussion

4.1 Impact of depth hoar on snow properties

The Ex_DH simulations that coupled the depth hoar process showed generally better agreements with the observed seasonal snow depth, compared to the underestimation by Ex_NODH (Fig. 2). Ex_DH produced a thicker snow depth (Fig. 2) that illustrates that the model suitably simulated the formation of less dense and loosely packed depth hoar crystals taking up more volume for the same amount of mass compared to denser, settled snowpack and the seasonal variability (Fig. 5). There was less difference in the simulated SWE, with Ex_NODH melting out slightly faster (Fig. 2b). The deeper snowpack with the Ex_DH simulations, compared to Ex_NODH, yet limited difference in SWE but sooner onset of melting illustrates the increased insulative

https://doi.org/10.5194/egusphere-2026-2767
Preprint. Discussion started: 11 August 2026

properties of the simulated depth hoar (Fig. 7) and difference in soil temperatures (Fassnacht and Soulis, 2002).

The snowpack with depth hoar had low snow densities less than 150 kg m^{-3} at the base in mid-winter (Suzuki et al., 2006), which was half to two-thirds of the snow density of the Ex_{NODH} simulated snowpack (Fig. 6). As the kinetic metamorphism is not modeled, the density in snowpacks generally increases with age, yielding bulk densities larger than observed (Fig. 6). The average snow density from October to February observed at taiga boreal forest regions over the Russian territory during the period of 1966–2008 was 130 to 200 kg m^{-3} (Zhong et al., 2014). In Alaska and the Canadian Arctic, the snowpack density with a basal depth hoar layer varied from 130 to 250 kg m^{-3} (Sturm et al., 1997; Domine et al., 2016). The simulated snow density is at the lower end of the observed ranges. The low snow density of the depth hoar led to low snow thermal conductivity of <0.1 W m^{-1} K^{-1} at the lower layers of snowpack (Fig. 7), which distributed within the range of 0.025–0.1 W m^{-1} K^{-1} obtained from various field observations (Sturm et al., 1997; Domine et al., 2016). The Ex_{DH}-simulated values of <0.1 W m^{-1} K^{-1} were 1.5 to 2 times lower than Ex_{NODH} (Fig. 7). The difference is not surprising if considering the dependence of the thermal conductivity on the snow density alone, as described in Eq. (2). Sturm and Johnson (1992) found that the thermal conductivity of depth hoar was approximately one-quarter to one-third that of snow layers with the same density, based on the field snow survey in Alaska. The observation and model simulation confirm the function of depth hoar as an insulator lowering snow thermal conductivity (Fig. 7).

The snow thermal conductivity schemes that are adapted by many land surface models tend to be more suitable for alpine conditions than Arctic environments (Damseaux et al., 2025). The climatic background inherent in the schemes likely becomes a source of uncertainty in simulations for different environments. Dutch et al. (2022) conducted a comparative analysis of different snow thermal conductivity schemes with CLM5.0 using in situ measurements from Northwest Territories, Canada, and found that the CLM5.0 default scheme overestimates snow thermal conductivity by a factor of 3 compared to the observations. The similar departures from observations were also found by simulations of different models (i.e., Crocus: Vionnet et al., 2012; SNOWPACK: Bartelt and Lehning, 2002; CLM5.0: Lawrence et al., 2019). To address this issue, some models incorporated the snow thermal conductivity scheme to the Sturm et al. (1997) equation derived from tundra snow conditions, which slightly improved the simulations (Paquin and Sushama, 2015; Barrere et al., 2017; Royer et al., 2021; Tao et al., 2024; Damseaux et al., 2025). The snow thermal conductivity of the Sturm equation was parameterized by snow density. Therefore, a misrepresentation in the modeling of snow density likely produces errors in the estimation of the snow thermal conductivity. A different approach considers the interactions between heat conduction and water vapor diffusion in the snowpack model to better simulate the snow thermal conductivity (Brondex et al., 2023).

4.2 Impact of depth hoar on soil temperature

The original simulation, Ex_{NODH}, produced cold biased soil temperatures compared to the observations, particularly in the wintertime (Fig. 3), as shown in other modeling studies (Dankers et al., 2011; Wang et al., 2013; Barrere et al., 2017; Guimberteau et al., 2018; Oogathoo et al., 2022). This current study reduced the cold biases based on a physical approach by

https://doi.org/10.5194/egusphere-2026-2767
Preprint. Discussion started: 11 August 2026

coupling a depth hoar scheme to the snow model. The improvement was demonstrated by smaller MAD and RMSE of Ex_DH compared to Ex_NODH (Fig. 3), as well as by the positive anomalies in the monthly averaged soil temperature between two simulations during the study period (Fig. 10). The anomalies were most pronounced during the winter months (Fig. 10) that the cold biases by Ex_NODH were significant (Fig. 3). Ex_DH reduced the cold biases by approximately 4°C at the top soil layer of 0–30 cm in February and by 2.5°C at the soil depth of 200–320 cm (Fig. 10).

The snow density in February showed a difference of approximately 100 kg m^{-3} between Ex_NODH and Ex_DH at the bottom snow layer (Fig. 6). The low snow density of snowpack, and thus decreased snow thermal conductivity, cooled the soil less, consequently warmer soil temperature. A density difference of 100 kg m^{-3} produced 2–4°C warmer soil temperatures (Fig. 10). The insulation of depth hoar also resulted in the soil temperatures being 0–1.5°C warming during the summer months (i.e., June–August, Fig. 10), which was linked to the increase of active layer thickness by 17 cm, on average, during the study period (Fig. 4). There are several numerical models to quantify the depth hoar impact on soil temperature. However, few modeling studies provided quantitative information related to the depth hoar effect. A sensitivity study using a one-dimensional heat transfer model changed the depth fraction of the depth hoar from 0 to 0.6 that increased the ground surface temperature by 12.8°C (Zhang et al., 1996). Yamazaki (2001) addressed the higher sensitivity of permafrost soil temperature on the depth hoar-formed snow cover in Yakutsk, eastern Siberia, based on the simulation by a model parameterizing depth hoar.

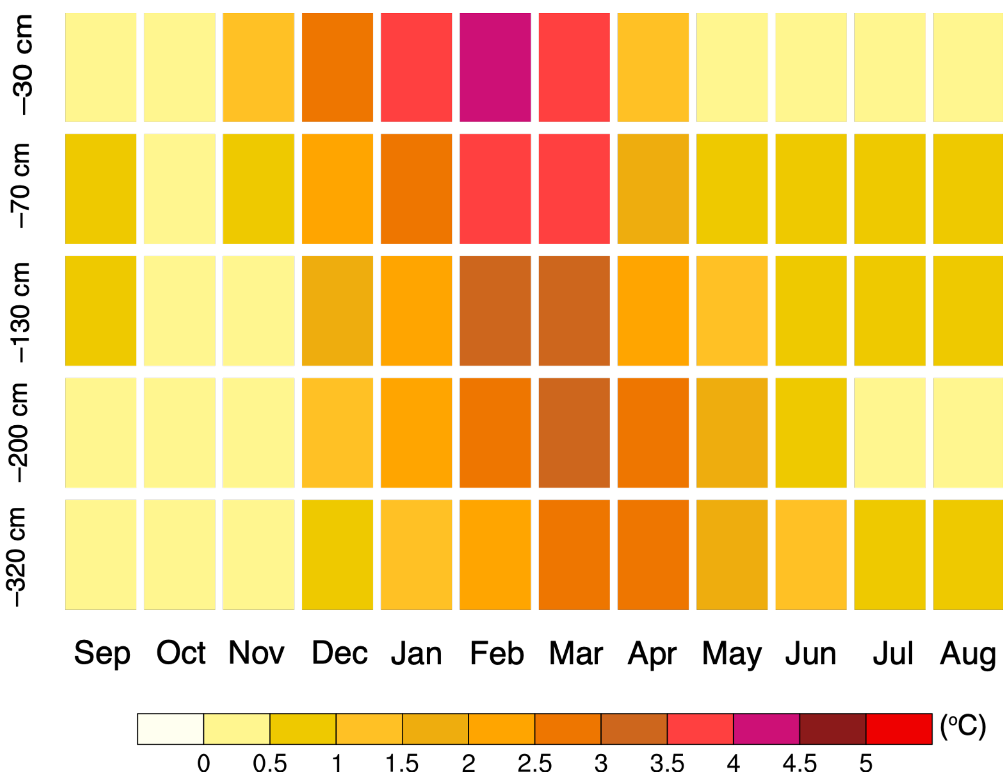

Figure 10. Period-averaged (1980–2016) differences in monthly soil temperature between the two experiments (Ex_NODH and Ex_DH).

https://doi.org/10.5194/egusphere-2026-2767
Preprint. Discussion started: 11 August 2026

Each row represents a different depth (0–30, 30–70, 70–130, 130–200, 200–320 cm), while each column represents the average of a different month.

The magnitude of snow insulation by depth hoar was most pronounced at the conditions for colder T_{air} and thicker snow depth (Fig. 8, 9). The snow density tends to be lower under cold T_{air} than warm due to metamorphism (Anderson, 1976), resulting in larger ΔT (higher snow insulation). Snow densification is also further rapid under cold temperatures, which increases thermal gradient of the snowpack, promoting the development of depth hoar (Zhang et al., 1996). Therefore, snow likely produces higher insulation in colder climates than in warmer ones. However, as snow depth exceeded 20 cm at the coldest T_{air} regime, $T_{air} \leq -25$°C, the median values of ΔT showed lower variability to the increase of snow depth (Fig. 8). This pattern was in line with previous findings based on in situ observations and modeling results (Zhang 2005; Wang et al., 2016; Slater et al., 2017; Damseaux et al., 2025). The cold T_{air} is an efficient condition for the formation and growth of depth hoar crystals in the snowpack. In practice, the model simulated continuously growing depth hoar layer during the winter months (Fig. 5). The thicker depth hoar layer under the increasing snow depth reduces heat loss from the soil to the atmosphere and thus lower sensitivity of ΔT to changes in snow depth. The analysis based on daily variations in soil surface temperature of Spasskaya Pad and snow depth observed at Yakutsk indicated that the snow insulating effect was effective when the snow depth was 10 cm or more (Iijima et al., 2010), which indirectly supports the appearance of depth hoar at that snow thickness. On the other hand, the interquartile range in ΔT vs snow depth most largely scattered under the coldest T_{air} regime, $T_{air} \leq -25$°C (Fig. 8). The scatter of the interquartile range resulted from the influence of cold T_{air} in the study site, characterized by large seasonal temperature cycle with greater interannual variability (Wang et al., 2016). This variability was also greatly related to the growth of the depth hoar, decoupling ΔT from snow depth and thereby increasing the scattering of the interquartile range. This study clearly underscores the efficiency of depth hoar as a good insulator, particularly under conditions of both colder T_{air} and thicker snow depth. This finding was in turn validated by additional simulations, forced by a meteorological dataset based on SSP 5.8.5 scenario of IPCC AR6, projected the future climatic changes. The difference in monthly soil temperature between $\mathrm{Ex\_}_{\mathrm{DH}}$ and $\mathrm{Ex\_}_{\mathrm{NODH}}$ under the warming future climate was averaged for the period of 2081–2100 (Fig. 11) and is consistent with in the period 1980–2016 (Fig. 10). The difference in soil temperatures between the two simulations was overall lower than in the present climate (Fig. 11). For example, the depth hoar in the future climate warmed the soil temperature of the surface layer (0–30 cm) by 2.5°C in February (Fig. 11), which was 1.5°C cooler than the present simulation (Fig. 10). This tendency was also found at the deeper soil layers. Owing to the warmer climates, the insulation magnitude of depth hoar in the future was lower than the present. However, the result shows that the depth hoar will play a role enhancing further the permafrost degradation under the future climate changes. Interestingly, the anomalous soil temperatures during the summer months (June to August) at the soil depth of 70–200 cm were 0.5~1.0°C warmer (Fig. 11) than the present (Fig. 10), which is attributed to the influence of the increased soil moisture at the soil layers (Figure S2), related to larger soil heat capacity.

https://doi.org/10.5194/egusphere-2026-2767
Preprint. Discussion started: 11 August 2026

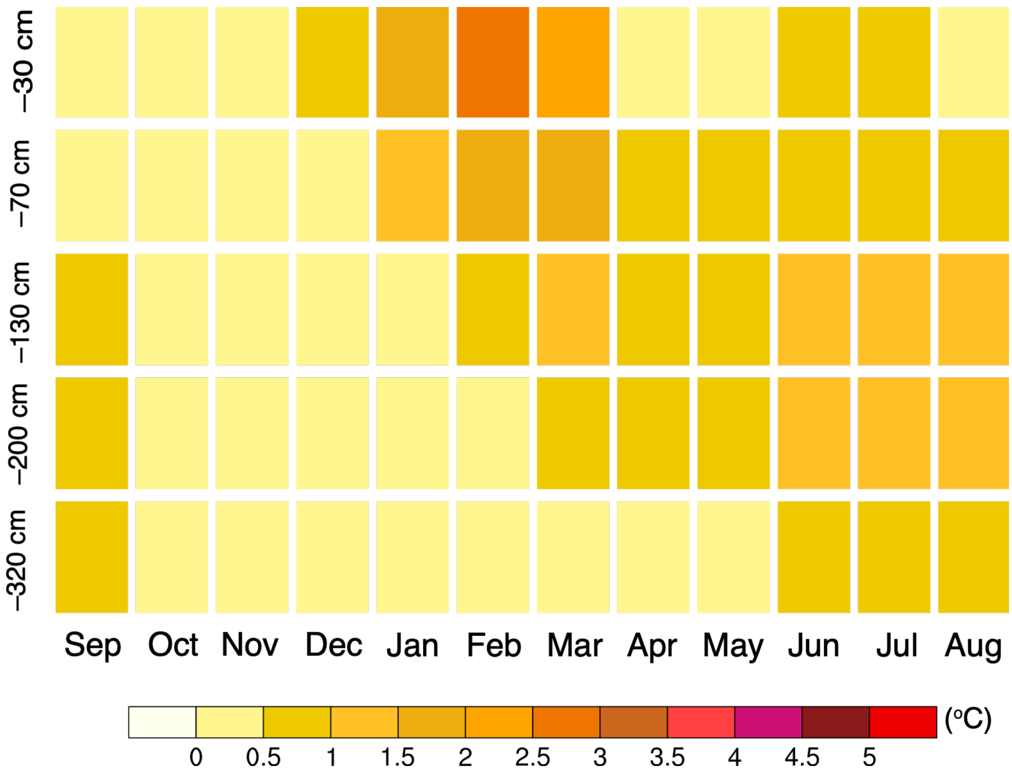

Figure 11. Period-averaged (2081–2100) differences in monthly soil temperature between the two experiments (Ex$_{_NODH}$ and Ex$_{_DH}$). Each row represents a different depth interval (0–30, 30–70, 70–130, 130–200, 200–320 cm), while each column represents the average of a different month. The simulations were forced by a meteorological dataset based on SSP 5.8.5 scenario of IPCC AR6, projected the future climatic changes.

4.3 Uncertainty and future work

The model that coupled the depth hoar process has produced clearly different profiles for the snow density (Fig. 6) and thus the snow thermal conductivity (Fig. 7), compared to the original simulation. In situ observations collected in the Arctic region presents snowpack profiles where the density generally decreased toward the basal layer of depth hoar, because the snowpack surface consists of a wind slab with a higher density, due to snow compaction from the strong Arctic wind transport and deposition (Sturm et al., 1995; Domine et al., 2018). Ex$_{_DH}$ simulated the snow density profiles similar to the observations in October and April (Fig. 6) when T_{air} was warmer and relatively wet snow was present. On the other hand, in the mid-winter months (i.e., December and February), Ex$_{_DH}$ produced the profiles of vertically homogeneous density (Fig. 6), which was different to the observations. The study site is defined as a continental climate characterized by cold T_{air} and less snowfall during the mid-winter season (Kotani et al., 2019). The wind is not stronger than in tundra regions, thus the snow deposition by blowing is infrequent. These climates are likely efficient for the development of depth hoar, probably reducing the difference in snow density between the surface and bottom layers in the snowpack. As shown in Fig. 5, the model simulated

https://doi.org/10.5194/egusphere-2026-2767
Preprint. Discussion started: 11 August 2026

vertically different features of metamorphic layers, showing the depth hoar layer growing over time. The profile of the vertical layers is similar to the metamorphic layers of different features observed in the subarctic snow cover, as illustrated in Fig. 5 of Sturm and Johnson (1992). However, the deficiency of snow survey data in the study site limits the evaluation of the simulated profiles of snow layers.

The $\mathrm{Ex\_}_{\mathrm{DH}}$ simulation reproduced the seasonal variability of soil temperatures observed at different soil depths well, improving upon the winter cold biases simulated by $\mathrm{Ex\_}_{\mathrm{NODH}}$ (Fig. 4). However, $\mathrm{Ex\_}_{\mathrm{DH}}$ still simulated cold and warm temperatures in the winter and summer, respectively, at the two soil depths (i.e., 30–70 cm and 70–130 cm) below the surface, compared to the observations. The lack in representing other insulative materials (e.g., moss/litter layer and soil organic carbon) is likely a partial cause of the discrepancy (Park et al., 2018). Another reason for this discrepancy is the impact of the underestimated soil moisture on soil temperature. The observed soil temperatures revealed longer zero curtain during the freezing and thawing seasons at the two soil depths (Fig. 4), due to latent heat fluxes from the phase change of soil moisture. Meanwhile, the model simulated faster freezing and thawing at the same seasons than the observed, with shorter zero curtain, which in part seems to be related to lower latent heat effect due to the underestimated soil moisture, particularly in the freezing season. On the other hand, the model simulated the early snow melting in the spring (Fig. 2). The observation was made at a forest different from the site for this study. Moreover, the observations of snow depth and SWE were the averaged values obtained at heterogeneous spaces along the 500 m and 2000 m courses (Zhong et al., 2014), while the simulation had a one-dimensional resolution for the study site. The divergent surface landscapes resulted from the different observational and modeling sites can primarily affect the inconsistency in the snowmelt timing. In particular, the difference in vegetation types does greatly influence radiation and energy fluxes and thus snowmelt. The model also calculated heat and water fluxes in the atmosphere–vegetation–snow–soil continuum based on radiation, energy, and water balances, in which a residual in the snow surface energy balance was forced as an input deriving heat transfer into the snow layers, interpolating the daily temporal resolution of meteorological forcing data to hourly time scales. In the transitional seasons, particularly in spring, the large diurnal or daily climate variability can occasionally produce large residual energy, enforcing snow melt. The influence is likely significant during thin and/or wet snowpack conditions. Toon et al. (1989) introduced a two-stream radiative transfer solution to estimate upward and downward radiative fluxes at each snow layer interface, from which net radiation, layer absorption, and surface albedo are easily derived. Many models that coupled the two-stream model have been implemented to enable prediction of radiative features in land surface processes, adding numerically efficient and modest costs (Best et al., 2011; Dai et al., 2003). The incorporation of a two-stream radiative scheme into the snow model is identified as an important development target for improving the model snow processes.

5 Conclusion

The CHANGE model that newly coupled the depth hoar scheme to the snowpack process allowed for simulations to quantify the impact of depth hoar on permafrost thermal regimes under the present and future climates in a boreal forest site. The simulated snow and soil thermal variables were compared with the field observations, which showed that the model

https://doi.org/10.5194/egusphere-2026-2767
Preprint. Discussion started: 11 August 2026

represented the seasonal and interannual variability of the observed snow depth, SWE, ALT, and soil temperature well statistically. The model simulations showed that the appearance of the depth hoar resulted in lower snow density less than 150 kg m^{-3} at the snowpack base in mid-winter and lower snow thermal conductivity of <0.1 W m^{-1} K^{-1} at the base, which reduced the cold bias by 2.5–4.0°C in the winter soil temperatures observed in the original simulation $Ex_{\_NODH}$ under the present climate. The warming effect remains into the summer season, resulting in more active layer thawing by up to 20 cm during the study period. The insulation efficiency of the depth hoar was further large under the conditions of colder T_{air} and thicker snow, which was demonstrated by both increased temperature difference between the air and soil depth at 20 cm with increasing snow depth under colder T_{air} conditions and a low correlation of soil temperature versus T_{air} under thicker snow. Moreover, depth hoar was also formed under the future warming climates and surface layer soil temperature warmed by 2.5°C in February. These results highlight the apparent role of depth hoar as an insulator deriving permafrost degradation in present and future climates. The depth hoar-induced permafrost warming and deepening active layer thickness appear to be influential in enhancing the melting of ground ice and decomposition of soil organic carbon within permafrost. These changes will have a broader range of connectivity with ecohydrological processes under the future climate changes, as well as positive feedback to climates. However, there have been few studies on how depth hoar influences permafrost thermal regimes and the associated processes. Further assessment to test the reality of our identified depth hoar depictions as an insulator is warranted as more observational data become available and model representations improve.

Data availability

Observational data and simulation results are available from Dataset used in the paper "Snowpack depth hoar impacts on the permafrost thermal regime in a land surface model"(10.5281/zenodo.21271559).

Author contributions

HP carried out the model experiments and evaluations and wrote the original draft of the paper, including the conceptualization of this study. TH and YI collected and analyzed the data for the model evaluation, and KS and SRF contributed to designing the model experiments. All authors developed the idea that led to this paper and were involved in the review and editing of the paper.

Competing interests

The contact author has declared that none of the authors has any competing interests.

https://doi.org/10.5194/egusphere-2026-2767
Preprint. Discussion started: 11 August 2026

Acknowledgements

The contact author acknowledges Dr. T. Yamazaki for contributing in the coding of depth hoar process.

Financial support

This work was conducted as part of the Japan Society for the Promotion of Science KAKENHI (grant number: 23K25012, 24H00125, 25H00507) and ArCS-3 (JPMXD1720251001).

References

Anderson, E. A.: A point energy and mass balance model of a snow cover, NOAA technical report NWS, 19, NOAA, Washington, DC, 150 pp., https://www.proquest.com/docview/302818861?pq-origsite=gscholar&fromopenview=true, 1976.

Barrere, M., Domine, F., Decharme, B., Morin, S., Vionnet, V., and Lafaysse, M.: Evaluating the performance of coupled snow–soil models in SURFEXv8 to simulate the permafrost thermal regime at a high Arctic site, Geosci. Model Dev., 10, 3461–3479, https://doi.org/10.5194/gmd-10-3461-2017, 2017.

Bartelt, P. and Lehning, M.: A physical SNOWPACK model for the Swiss avalanche warning, Cold Reg. Sci. Technol., 35, 123–145, https://doi.org/10.1016/S0165-232X(02)00074-5, 2002.

Best, M. J., Pryor, M., Clark, D. B., Rooney, G. G., Essery, R. L. H., Ménard, C. B., Edwards, J. M., Hendry, M. A., Porson, A., Gedney, N., Mercado, L. M., Sitch, S., Blyth, E., Boucher, O., Cox, P. M., Grimmond, C. S. B., and Harding, R. J.: The Joint UK Land Environment Simulator (JULES), model description – Part 1: Energy and water fluxes, Geosci. Model Dev., 4, 677–699, https://doi.org/10.5194/gmd-4-677-2011, 2011.

Brondex, J., Fourteau, K., Dumont, M., Hagenmuller, P., Calonne, N., Tuzet, F., and Löwe, H.: A finite-element framework to explore the numerical solution of the coupled problem of heat conduction, water vapor diffusion, and settlement in dry snow (IvoriFEM v0.1.0), Geosci. Model Dev., 16, 7075–7106, https://doi.org/10.5194/gmd-16-7075-2023, 2023.

Colbeck, S. C.: Theory of metamorphism of dry snow, J. Geophys. Res. Oceans Atmos., 88(NC9), 5475–5482, 1983.

Dai, Y., Zeng, X., Dickinson, R., Baker, I., Bonan, G., Bosilovich, M., et al.: The common land model, Bullet. Am. Meteorol. Soc., 84(8), 1013–1024. https://doi.org/10.1175/bams-84-8-1013, 2003.

Damseaux, A., Matthes, H., Dutch, V. R., Wake, L., and Rutter, N.: Impact of snow thermal conductivity schemes on pan-Arctic permafrost dynamics in the Community Land Model version 5.0, The Cryosphere, 19, 1539–1558, https://doi.org/10.5194/tc-19-1539-2025, 2025.

Dankers, R., Burke, E. J., and Price, J.: Simulation of permafrost and seasonal thaw depth in the JULES land surface scheme, The Cryosphere, 5, 773–790, https://doi.org/10.5194/tc-5-773-2011, 2011.

Domine, F., Gallet, J.-C., Bock, J., and Morin, S.: Structure, specific surface area and thermal conductivity of the snowpack around Barrow, Alaska. J. Geophys. Res., 117, D00R14, https://doi.org/10.1029/2011jd016647, 2012.

Domine, F., Barrere, M., and Sarrazin, D.: Seasonal evolution of the effective thermal conductivity of the snow and the soil in high Arctic herb tundra at Bylot Island, Canada. Cryosphere, 10, 2573–2588, https://doi.org/10.5194/tc-10-2573-2016, 2016.

Domine, F., Belke-Brea, M., Sarrazin, D., Arnaud, L., Barrere, M., and Poirier, M.: Soil moisture, wind speed and depth hoar formation in the Arctic snowpack, J. Glaciol., 64, 990–1002, https://doi.org/10.1017/jog.2018.89, 2018.

Domine, F., Picard, G., Morin, S., Barrere, M., Madore, J.-B., and Langlois, A.: Major Issues in Simulating Some Arctic Snowpack Properties Using Current Detailed Snow Physics Models: Consequences for the Thermal Regime and Water Budget of Permafrost, J. Adv. Model. Earth Sy., 11, 34–44, https://doi.org/10.1029/2018MS001445, 2019.

Dutch, V. R., Rutter, N., Wake, L., Sandells, M., Derksen, C., Walker, B., Hould Gosselin, G., Sonnentag, O., Essery, R., Kelly, R., Marsh, P., King, J., and Boike, J.: Impact of measured and simulated tundra snowpack properties on heat transfer, The Cryosphere, 16, 4201–4222, https://doi.org/10.5194/tc-16-4201-2022, 2022.

Ekici, A., Beer, C., Hagemann, S., Boike, J., Langer, M., Hauck, C.: Simulating high-latitude permafrost regions by the JSBACH terrestrial ecosystem model, Geosci. Model Dev., 7, 631–647, https://doi.org/10.5194/gmd-7-631-2014, 2014.

Estilow, T. W., Young, A. H., and Robinson, D. A.: A long-term Northern Hemisphere snow cover extent data record for climate studies and monitoring. Earth Syst. Sci. Data, 7, 137–142, doi:10.5194/essd-7-137-2015, 2015.

Fassnacht, S. R., and Soulis, E. D.: Implications during transitional periods of improvements to the snow processes in the Land Surface Scheme – Hydrological Model WATCLASS, Atmosphere-Ocean, 40(4), 389–403, https://doi.org/10.3137/ao.400402, 2002.

Fukuzawa, T., and Akitaya, E.: An experimental study on the growth rates of depth hoar crystals at high temperature gradients (I), Low Temp. Sci. Ser., A 50, 9–14, 1991. (in Japanese with English summary)

Guimberteau, M., Zhu, D., Maignan, F., Huang, Y., Yue, C., Dantec-Nédélec, S., Ottlé, C., Jornet-Puig, A., Bastos, A., Laurent, P., Goll, D., Bowring, S., Chang, J., Guenet, B., Tifafi, M., Peng, S., Krinner, G., Ducharne, A., Wang, F., Wang, T., Wang, X., Wang, Y., Yin, Z., Lauerwald, R., Joetzjer, E., Qiu, C., Kim, H., and Ciais, P.: ORCHIDEE-MICT (v8.4.1), a land surface model for the high latitudes: model description and validation, Geosci. Model Dev., 11, 121–163, https://doi.org/10.5194/gmd-11-121-2018, 2018.

Hinkel, K. M., and Hurd, J. K.: Permafrost destabilization and thermokarst following snow fence installation, Barrow, Alaska, U.S.A. Arctic Antarctic and Alpine Research, 38(4), 530–539, https://doi.org/10.1657/1523-0430(2006)38[530:PDATFS]2.0.CO;2, 2006.

Hirashima, H., Abe, O., Sato, A., and Lehning, M.: Implementation of depth hoar factor into the SNOWPACK model, Int. Snow Sci. Workshop, 970–977, 2008.

Iijima, Y., Fedorov, A. N., Park, H., Suzuki, K., Yabuki, H., Maximov, T. C., and Ohata, T.: Abrupt increases in soil temperatures following increased precipitation in a permafrost region, central Lena River Basin, Russia, Permafr. Periglac. Process., 21(1), 30–41, https://doi.org/10.1002/ppp.662, 2010.

Iijima, Y., Nakamura, T., Park, H., Tachibana, Y., and Fedorov, A.: Enhancement of Arctic storm activity in relation to permafrost degradation in eastern Siberia, Int. J. Climatol., 36, 4265–4275, https://doi.org/10.1002/joc.4629, 2016.

IPCC, Climate Change 2022: Impacts, Adaptation, and Vulnerability. Contribution of Working Group II to the Sixth Assessment Report of the Intergovernmental Panel on Climate Change, H.-O. P.rtner, D. C. Roberts, M. Tignor, E. S. Poloczanska, K. Mintenbeck, A. Alegr.a, M. Craig, S. Langsdorf, S. L.schke, V. M.ller, A. Okem, B. Rama, Eds. (Cambridge Univ. Press, 2022).

Jordan, R. E.: A one-dimensional temperature model for a snow cover: Technical documentation for SNTHERM. 89., Cold Regions Research and Engineering Laboratory (U.S.) Engineer Research and Development Center (U.S.), https://erdc-library.erdc.dren.mil/jspui/handle/11681/11677, 1991.

Kim, Y., Kimball, J. S., Glassy, J., and Du, J.: An extended global earth system data record on daily landscape freeze-thaw status determined from satellite passive microwave remote sensing. Earth Syst. Sci. Data 9, 133–147, https://doi.org/10.5194/essd-9-133-2017, 2017.

Kojima, K.: Viscous compression of natural snow layers II, Low Temperature Science, Ser. A 15, 117–135, 1956. (in Japanese with English summary)

Kojima, K.: Viscous compression of natural snow layers III. Low Temperature Science, Ser. A 16, 167–196, 1957. (in Japanese with English summary)

Kojima, K.: Densification of seasonal snow cover, Proc. International Conference on Low Temperature Science, August 14–19, 1966, Sapporo, Japan, 929–952, 1967.

Kotani, A., Saito, A., Kononov, A. V., Petrov, R. E., Maximov, T. C., Iijima, Y., and Ohta, T.: Impact of unusually wet permafrost soil on understory vegetation and CO2 exchange in a larch forest in eastern Siberia, Agr. For. Meteorol., 265, 295–309, https://doi.org/10.1016/j.agrformet.2018.11.025, 2019.

Lawrence, D. M., Slater, A. G., and Swenson, S. C.: Simulation of Present-Day and Future Permafrost and Seasonally Frozen Ground Conditions in CCSM4, J. Climate, 25, 2207–2225, 2012.

Lawrence, D. M., Fisher, R. A., Koven, C. D., et al.: The Community Land Model Version 5: Description of New Features, Benchmarking, and Impact of Forcing Uncertainty, J. Adv. Model. Earth Sy., 11, 4245–4287, https://doi.org/10.1029/2018MS001583, 2019.

Luo, Z., Risto, D., and Ahrens, B.: Assessing uncertainties in modeling the climate of the Siberian frozen soils by contrasting CMIP6 and LS3MIP, The Cryosphere, 19, 6547–6576, https://doi.org/10.5194/tc-19-6547-2025, 2025.

Marbouty, D.: An experimental study of temperature-gradient metamorphism. J. Glaciol., 26(94), 303–312, 1980.

McCrystal, M. R., Stroeve, J., Serreze, M., Forbes, B. C., and Screen, J. A.: New climate models reveal faster and larger increases in Arctic precipitation than previously projected. Nat. Commun. 12, 6765, 2021.

Mudryk, L. R., Kushner, P. J., Derksen, C., and Thackeray, C.: Snow cover response to temperature in observational and climate model ensembles, Geophys. Res. Lett., 44, 919–926, https://doi.org/10.1002/2016GL071789, 2017.

Mudryk, L., Santolaria-Otín, M., Krinner, G., Ménégoz, M., Derksen, C., Brutel-Vuilmet, C., Brady, M., and Essery, R.: Historical Northern Hemisphere snow cover trends and projected changes in the CMIP6 multi-model ensemble. Cryosphere 14, 2495–2514, 2020.

Miyazaki, S., Saito, K., Mori, J., Yamazaki, T., Ise, T., Arakida, H., et al.: The GRENE-TEA model intercomparison project (GTMIP): Overview and experiment protocol for stage 1, Geosci. Model Dev., 8, 2841–2856, https://doi.org/10.5194/gmd-8-2841-2015, 2015.

O'Gorman, P. A.: Contrasting responses of mean and extreme snowfall to climate change, Nature, 512, 416–418, 2014.

Oogathoo, S., Houle, D., Duchesne, L., and Kneeshaw, D.: Evaluation of simulated soil moisture and temperature for a Canadian boreal forest, Agr. Forest Meteorol., 323, 109078, https://doi.org/10.1016/j.agrformet.2022.109078, 2022.

Paquin, J.-P. and Sushama, L.: On the Arctic near-surface permafrost and climate sensitivities to soil and snow model formulations in climate models, Clim. Dyn., 44, 203–228, https://doi.org/10.1007/s00382-014-2185-6, 2015.

Park, H., Iijima, Y., Yabuki, H., Ohta, T., Walsh, J., Kodama, Y., and Ohata, T.: The application of a coupled hydrological and biogeochemical model (CHANGE) for modeling of energy, water, and CO2 exchanges over a larch forest in eastern Siberia, J. Geophys. Res., 116, D15102, https://doi.org/10.1029/2010JD015386, 2011.

Park, H., Walsh, J., Fedorov, A. N., Sherstiukov, A. B., Iijima, Y., and Ohata, T.: The influence of climate and hydrological variables on opposite anomaly in active-layer thickness between Eurasian and north American watersheds, The Cryosphere, 7, 631–645, https://doi.org/10.5194/tc-7-631-2013, 2013.

Park, H., Fedorov, A. N., Zheleznyak, M. N., Konstantinov, P. Y., and Walsh, J. E.: Effect of snow cover on pan-Arctic permafrost thermal regimes, Clim. Dyn., 44, 2873–2895, https://doi.org/10.1007/s00382-014-2356-5, 2015.

Park, H., Launiainen, S., Konstantinov, P. Y., Iijima, Y., and Fedorov, A. N.: Modeling the effect of moss cover on soil temperature and carbon fluxes at a tundra site in northeastern Siberia, J. Geophys. Res.: Biogeos., 123, 3028–3044, https://doi.org/10.1029/2018JG004491, 2018

Park, H., Tanoue, M., Sugimoto, A., Ichiyanagi, K., Iwahana, G., and Hiyama, T.: Quantitative separation of precipitation and permafrost waters used for evapotranspiration in a boreal forest: a numerical study using tracer model, J. Geophys. Res.: Biogeos., 126, e2021JG006645, https://doi.org/10.1029/ 2021JG006645, 2021.

Park, H., Kim, Y., Suzuki, K., Hiyama, T.: Influence of snowmelt on increasing Arctic river discharge: numerical evaluation, Prog. Earth Planet. Sci., 11, 13, https://doi.org/10.1186/s40645-024-00617-y, 2024.

Park, H., Kim, Y., Gibson, J., and Hiyama, T.: Water tracer model-assessed contributions of source waters to changing circumpolar Arctic terrestrial evapotranspiration and river discharge, J. Hydrol., 664, 134379, https://doi.org/10.1016/j.jhydrol.2025.134379, 2026.

Pongracz, A., Wårlind, D., Miller, P. A., Gustafson, A., Rabin, S. S., and Parmentier, F.-J. W.: Warming-induced contrasts in snow depth drive the future trajectory of soil carbon loss across the Arctic-Boreal region, Commun. Earth Environ., 5, 684, https://doi.org/10.1038/s43247-024-01838-1, 2024.

Pulliainen, J., Luojus, K., Derksen, C. *et al.*: Patterns and trends of Northern Hemisphere snow mass from 1980 to 2018, Nature 581, 294–298, https://doi.org/10.1038/s41586-020-2258-0, 2020.

https://doi.org/10.5194/egusphere-2026-2767
Preprint. Discussion started: 11 August 2026

Royer, A., Picard, G., Vargel, C., Langlois, A., Gouttevin, I., and Dumont, M.: Improved Simulation of Arctic Circumpolar Land Area Snow Properties and Soil Temperatures, Front. Earth Sci., 9, 685140, https://doi.org/10.3389/feart.2021.685140, 2021.

Shinojima, K.: Study on the Visco-Elastic deformation of deposited snow, H. Oura, Ed., *Physics of Snow and Ice*, Vol. I(2), Inst. Low Temp. Sci. Hokkaido Univ., 875–907, 1967.

Slater, A. G., Lawrence, D. M., and Koven, C. D.: Process level model evaluation: a snow and heat transfer metric, The Cryosphere, 11, 989–996, https://doi.org/10.5194/tc-11-989-2017, 2017.

Sturm, M., Holmgren, J., and Liston, G. E.: A seasonal snow cover classification-system for local to global applications, J. Clim., 8(5), 1261–1283, 1995.

Sturm, M., Holmgren, J., König, M., and Morris, K.: The thermal conductivity of seasonal snow, J. Glaciol., 43, 26–41, https://doi.org/10.3189/S0022143000002781, 1997.

Sturm, M., and Johnson, J. B.: Natural-convection in the sub-arctic snow cover, J. Geophys. Res. Solid Earth Planets, 96(B7), 11657–11671, 1991.

Sturm, M., and Johnson, J. B.: Thermal Conductivity Measurements of Depth Hoar. J. Geophys. Res. 97(B2), 2129-2139, 1992.

Suzuki, K., Kubota, J., Zhang, Y., Kadota, T., Ohata, T., and Vuglinsky, V.: Snow ablation in an open field and larch forest of the southern mountainous region of eastern Siberia, Hydrological Science Journal, 51:3, https://doi.org/10.1623/hysj.51.3.465, 2006.

Tao, J., Riley, W. J., and Zhu, Q.: Evaluating the impact of peat soils and snow schemes on simulated active layer thickness at pan-Arctic permafrost sites, Environ. Res. Lett., 19, 054027, https://doi.org/10.1088/1748-9326/ad38ce, 2024.

Toon, O. B., McKay, C. P., Ackerman, T. P., and Santhanam, K.: Rapid calculation of radiative heating rates and photodissociation rates in inhomogeneous multiple scattering atmospheres, J. Geophys. Res., 94(D13), 16287–16301, https://doi.org/10.1029/JD094iD13p16287, 1989.

Vionnet, V., Brun, E., Morin, S., Boone, A., Faroux, S., Le Moigne, P., Martin, E., and Willemet, J.-M.: The detailed snowpack scheme Crocus and its implementation in SURFEX v7.2, Geosci. Model Dev., 5, 773–791, https://doi.org/10.5194/gmd-5-773-2012, 2012.

Walker, M. D., Walker, D. A., Welker, J. M., Arft, A., Bardsley, T., Brooks, P., et al.: Long-term experimental manipulation of winter snow regime and summer temperature in arctic and alpine tundra. Hydrol. Process., 13(14–15), 2315–2330, https://doi.org/10.1002/(sici)1099-1085(199910)13:14/15<2315::aid-hyp888>3.0.co;2-a, 1999.

Wang, T., Ottlé, C., Boone, A., Ciais, P., Brun, E., Morin, S., Krinner, G., Piao, S., and Peng, S.: Evaluation of an improved intermediate complexity snow scheme in the ORCHIDEE land surface model, J. Geophys. Res.-Atmos., 118, 6064–6079, https://doi.org/10.1002/jgrd.50395, 2013.

Wang, W., Rinke, A., Moore, J. C., Ji, D., Cui, X., Peng, S., Lawrence, D. M., McGuire, A. D., Burke, E. J., Chen, X., Decharme, B., Koven, C., MacDougall, A., Saito, K., Zhang,W., Alkama, R., Bohn, T. J., Ciais, P., Delire, C., Gouttevin, I.,

https://doi.org/10.5194/egusphere-2026-2767
Preprint. Discussion started: 11 August 2026

Hajima, T., Krinner, G., Lettenmaier, D. P., Miller, P. A., Smith, B., Sueyoshi, T., and Sherstiukov, A. B.: Evaluation of air–soil temperature relationships simulated by land surface models during winter across the permafrost region, The Cryosphere, 10, 1721–1737, https://doi.org/10.5194/tc-10-1721-2016, 2016.

Yamazaki, T.: A one-dimensional land surface model applicable to intensely cold regions and its applications in eastern Siberia, J. Meteorol. Soc. Jpn., 79(6), 1107–1118, 2001.

Yamazaki, T., Sakuraoka, T., Nakamura, T., and Kondo, J.: A one-dimensional model of the evolution of snow-cover characteristics, Annals Glaciol., 18, 22–26, 1993.

Yosida, Z.: Physical studies on deposited snow, 1, thermal properties, Contribs. Inst. Low Temp. Sci., Hokkaido Univ., Japan, 7, 19–74, 1955.

Zhang, T.: Influence of the seasonal snow cover on the ground thermal regime: an overview. Rev. Geophys., 43(4), RG4002, https://doi.org/10.1029/2004rg000157, 2005.

Zhang, T., Osterkamp, T. E., and Stamnes, K.: Influence of the depth hoar layer of the seasonal snow cover on the ground thermal regime, Water Resour. Res., 32, 2075–2086, https://doi.org/10.1029/96wr00996, 1996.

Zhong, X., Zhang, T., Kang, S., Wang, K., Zheng, L., Hu, Y., and Wang, H.: Spatiotemporal variability of snow depth across the Eurasian continent from 1966 to 2012. The Cryosphere, 12, 227–245, https://doi.org/10.5194/tc-12-227-2018, 2018.

Zhu, X., Lee, S.-Y., Wen, X., Wei, Z., Ji, Z., Zheng, Z., and Dong, W.: Historical evolution and future trend of Northern Hemisphere snow cover in CMIP5 and CMIP6 models, Environ. Res. Lett. 16, 065013, 2021.